Charge degrees of freedom in frustrated lattice structures

Erich Runge
Technische Universität Ilmenau, Fakultät für Mathematik und Naturwissenschaften, FG Theoretische Physik I, 98693 Ilmenau, Germany

Peter Fulde
Max-Planck-Institut für Physik komplexer Systeme, Nöthnitzer-Strasse 38, 01187 Dresden, Germany
(Received 5 March 2004; published 15 December 2004)

We study numerically spinless fermions with strong nearest-neighbor repulsion V on frustrated lattice structures that show macroscopically many ground states in the absence of a kinetic energy term (hopping term). A finite hopping amplitude t lifts the macroscopic degeneracy and leads to a small number of degenerate ground states. These can be characterized by topological quantum numbers and transformation properties under symmetry operations such as particle-hole interchange. Results for the criss-crossed checkerboard lattice (two-dimensional pyrochlore lattice) with up to 32 fermions support the scenario that translational invariance is restored in the thermodynamic limit, making half-charged quasiparticles possible. A finite entropy of approximately $(3/4)\ln(4/3)$ per site is released at low temperatures $k_BT \approx t^3/V^2$, much below the bare energies t, V. This is familiar from the widely studied models involving spins on frustrated lattices, but in a spinless-fermion model these low-energy excitations are necessarily related to charge degrees of freedom.

DOI: 10.1103/PhysRevB.70.245113 PACS number(s): 71.27.+a, 71.10.Fd, 71.10.Pm

I. INTRODUCTION

Systems with frustrated lattice structures may show fascinating physical properties.[1] Therefore it is of no surprise that interest in them has been steadily increasing. A well known three-dimensional frustrated structure is the pyrochlore lattice. It consists of corner-sharing tetrahedra. For example, the sites A as well as the B sites of compounds $A_2B_2O_7$, where A is a large and B is a small ion, e.g., $Y_2Ru_2O_7$, form a pyrochlore lattice as do the so-called B sites of spinels. Examples of two-dimensional frustrated lattice structures are the checkerboard lattice, the kagomé lattice, and the triangular lattice. A pyrochlore lattice can be considered as a sequence of alternating planes of kagomé and triangular lattices. One may also think of the checkerboard lattice as a two-dimensional projection of a pyrochlore lattice. This explains why a checkerboard lattice is often considered in theoretical studies instead of the more realistic pyrochlore structure.

Frustrated lattices have their name because when a spin is attached to each of the sites, an antiferromagnetic spin interaction leads to frustrated spin-spin couplings. This may result in ground states without magnetic long-range order, i.e., in spin liquid states. This is the reason why a large amount of literature deals with frustrated spin lattices;[1–3] see, e.g., Refs. 4–8 and references therein for different aspects. In comparison with spin problems, charge degrees of freedom in frustrated lattices have obtained comparatively little attention. An exception is the investigation of electronic charge order in systems like magnetite Fe_3O_4.[9,10] The very fact that charge order has been observed in several pyrochlore lattices, not only in Fe_3O_4 but also in LiV_2O_4 under pressure[11] or AlV_2O_4,[12] suggests that electron correlations are strong in some of those systems. Most noticeable, heavy-fermion behavior has been found in the d-metal compound LiV_2O_4 under ambient pressure.[13] The origin of the heavy mass, i.e., the high density of low-lying fermionic degrees of freedom, is hotly debated at present.[14] In these systems, it is not sufficient to treat those correlations by an on-site Hubbard interaction parameter U only. For example, in the case of Fe_3O_4 that would merely restrict the Fe configurations on the spinel B sites to $3d^5$ and $3d^6$ and would not inhibit motion of an electron from a d^6 to a d^5 site. In order to suppress those motions a strong interaction between neighboring sites is required. From the work of Verwey,[15] who tried to explain the metal-insulator transition studied by him and Haayman,[10] and in particular from that of Anderson,[16] it is known that the nearest-neighbor Coulomb repulsions in Fe_3O_4 are minimized if on each tetrahedron two sites are in a $3d^5$ and two in a $3d^6$ configuration. This is called the *tetrahedron rule*, abbreviated τ rule henceforth. It explains why the observed entropy reduction at the metal-insulator transition in Fe_3O_4 is much less than expected from electrons without the strong short-range correlation. More recently the applicability of the τ rule to magnetite has been questioned because of the involvement of lattice degrees of freedom in that transition.[17] These are of no concern for the model Hamiltonian considered here.

More generally, the tetrahedron rule requires that for a pyrochlore lattice with a half-integer number of electrons per site two of the sites on a tetrahedron are occupied with ions of one valency and two with ions of the other valency, e.g., 0 and 1 valence electron or 1 and 2 valence electrons, etc. This can be done in many different ways and the classical ground state is therefore highly degenerate.

The above arguments assume that the kinetic or hopping energy of the electrons is negligible. In reality it will lift the high degeneracy of the ground state. How this occurs and to which low-energy excitations it leads have remained open questions. The problem is addressed in this paper by means

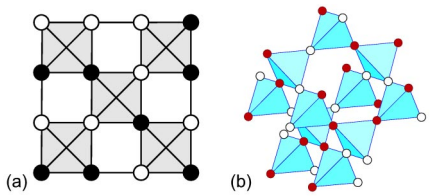

FIG. 1. (Color online) Half-filled checkerboard lattice (a) of spinless fermions as two-dimensional model of the half-filled pyrochlore lattice (b). Filled (hollow) symbols signify occupied (empty) sites. The configurations shown obey the respective tetrahedron rule in two or three dimensions.

of numerical calculations for a checkerboard lattice. In Ref. 18, it was pointed out that the near-degeneracy of the ground state in the presence of small hopping matrix elements can give raise to excitations with charges $\pm e/2$. By means of numerical methods on small systems we want to investigate here how this suggestion can be more substantiated. Again, we shall use a checkerboard lattice for this study. Furthermore, for simplicity we shall use spinless fermions or what is equivalent, a fully polarized electronic system with 0.5 electrons per site. Particular emphasis will be put on the ground state and the reduction of its degeneracy by a small kinetic energy term.

The paper is organized as follows: In the next section we introduce the Hamiltonian and present some computational considerations. An effective Hamiltonian is derived for the checkerboard lattice, which includes the effects of the kinetic energy by means of ring-hopping processes. It acts only on configurations that satisfy the tetrahedron rule. Furthermore, it is demonstrated that topological quantum numbers may be introduced that simplify computations and allow for deeper insight into the nature of the low-energy excitations. Extensive numerical calculations are presented in Sec. III. The use of the effective Hamiltonian is justified by comparison with results from diagonalization of the full problem. For the effective Hamiltonian, rather large systems with up to, 8×8 sites and 32 fermions can be studied on a single 64-bit workstation with a few gigabyte memory. This refers to the determination of the low-energy states, the density of states, the specific heat, and the nature of the ground states. The participation ratio is introduced as a convenient characterization of how many configuration contribute to a given eigenstate. In every case considered, a small number of degenerate ground states is found. In general, the corresponding charge densities are not translational invariant. However, Sec. III E presents arguments that suggest that the broken translational symmetry is a finite size effect and that a "disordered" translational invariant liquid ground state is found in the thermodynamic limit. The last section, Sec. IV contains the conclusions and addresses some open questions.

II. CHECKERBOARD LATTICE WITH NEAREST-NEIGHBOR REPULSION

We consider in the following a checkerboard lattice (see Fig. 1) with spinless fermions. Instead of spinless fermions,

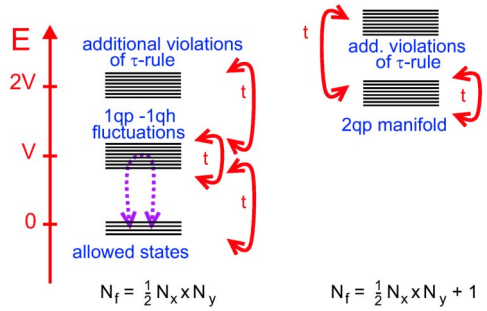

FIG. 2. (Color online) Illustration of the different subspace relevant for the calculation of low-energy properties of the half-filled (left) and slightly doped (right) checkerboard lattice with nearest-neighbor repulsion V. There are no matrix elements of the kinetic energy between different allowed states. These are, however, connected by virtual processes involving one-quasiparticle–one quasihole configurations as intermediate states.

one can also think of fully spin-polarized electrons. Double occupancies of sites are forbidden this way. Furthermore, a repulsive interaction V between fermions on neighboring sites is assumed. This includes interactions along the diagonals because in a three-dimensional pyrochlore lattice those diagonals connect nearest-neighbor sites. The Hamiltonian that we shall use is of the form

$$H = -t\sum_{\langle ij\rangle} (c_i^\dagger c_j + \text{H.c.}) + V\sum_{\langle ij\rangle} n_i n_j. \tag{1}$$

The $c_i^\dagger(c_i)$ denote creation (annihilation) operators at site i, and $\langle ij\rangle$ refers to a pair of nearest-neighbor sites. Furthermore, $n_i = c_i^\dagger c_i$. The fermionic character of the particles makes the present model fundamentally different from related spin models and related models for hard-core bosons.[1,3,4,6–8,14,19–26] Furthermore, the fermionic minus-sign problem excludes the use of quantum Monte Carlo methods that have been applied successfully to quite large spin and boson systems.

The momentum-dependent noninteracting $(V=0)$ dispersions of the criss-crossed checkerboard lattice are given by

$$\epsilon^-(\mathbf{k}) = -2t - 4t\cos\frac{k_x a}{\sqrt{2}}\cos\frac{k_y a}{\sqrt{2}}, \tag{2a}$$

$$\epsilon^+(\mathbf{k}) = 2t, \tag{2b}$$

where a is the lattice constant. There are two sites per unit cell. The occurrence of at least one flat band $\epsilon^+(\mathbf{k})$ is a characteristic feature of corner-connected complete graphs.[27] In general, a strong asymmetry $t \leftrightarrow -t$ is expected on the single-particle level when either the dispersive band $(t>0)$ or the dispersionless one $(t<0)$ is partially filled. The asymmetry is not present in the exactly half-filled interacting case. This may come as a surprise because in the single-particle picture the filled levels are quite different, but follows from particle-hole symmetry.

A. Tetrahedron rule and relevant subspaces

We are interested in the limit of large intersite repulsions V, i.e., when $t/V \ll 1$. In that case the tetrahedron (τ) rule is a very useful concept. As pointed out above it was suggested in order to explain the observed metal-insulator phase transition in Fe_3O_4. The τ rule implies for half-filling that on each tetrahedron of a pyrochlore lattice or criss-crossed square of a checkerboard lattice two sites are occupied and two sites remain empty. This way the Coulomb repulsion term in Eq. (1) is minimized.

Having in mind numerical calculation in the large-V limit, we decompose the full Hilbert space of all configurations into subspaces of given particle number and given number of τ-rule violations (see Fig. 2).

Many different configurations satisfy the tetrahedron rule, i.e., when $t=0$ the ground state of the system is highly degenerate; for an illustration, see Fig. 11 below. We will refer to these states as spanning the *allowed subspace*. As regards counting configurations, the half-filled rectangular checkerboard lattice of $N_x \times N_y$ sites with

$$N_f = \frac{1}{2} N_x N_y \tag{3}$$

identical particles can be mapped to the so-called ice problem with degeneracy[28]

$$N_{\mathrm{deg}} \simeq (4/3)^{(3/4)N_x N_y}. \tag{4}$$

The action of the kinetic energy term in Eq. (1) depends, of course, on the nature of the considered particles (fermions or bosons). Hopping generates configurations that are outside the allowed subspace. The τ rule is violated on two tetrahedra (or criss-crossed squares) that have excess τ charges of 1 and -1. When $t \ll V$, we may consider these configurations as vacuum fluctuations or, more generally as one-quasiparticle–one-quasihole (1qp-1qh) excitations. The net energy cost is V, but there is a gain in kinetic $\sim t$ associated with them, i.e.,

$$E_{\mathrm{1qp\text{-}1qh}} = V - O(t). \tag{5}$$

We use the quasiparticle-hole language because it suggests that the two defects can separate over large distances and have to be considered as entities of their own. This is described in more detail in Ref. 18, but for the purpose of the present paper 1qp-1qh simply is a label for a certain subspace of states. Configurations with additional τ-rule violations have even higher energies.

The degeneracy of the allowed manifold will be lifted at finite kinetic energy t by admixing fluctuations, which connect different classically degenerate allowed states. This suggests the following scenario: At finite hopping, the allowed manifold spreads over an energy regime characterized by a small energy that one might expect to be $\propto t^2/V$, but which is actually found to be $\propto t^3/V^2$ due to a subtle cancellation resulting from the fermionic anticommutation rules (see below). The much larger subspace of vacuum fluctuations starts at higher energies $E \approx V$. States within that subspace are directly connected by the hopping term in Eq. (1). Thus, an energy width $\propto t$ is expected [see Eq. (5)]. These considerations suggest a phase transition when t is of the order of V. More specifically, one may expect metallic behavior in the limit $V \to 0$. However, this limit may be singular because as noted before the half-filled case separates two very different bands in the noninteracting dispersion (2).

Our interest in the checkerboard lattice with nearest-neighbor interaction is motivated by the possibility of fractional charges in the slightly doped case with, e.g., one extra fermion. Again, configurations can be classified according to the number of τ-rule violations. One expects[18] [see Fig. 2(b)] a low-energy manifold of states with exactly two violations, each having a τ charge of 1. Some fermions in the vicinity of these two "defects" can now hop without additional τ-rule violations and lower their energy $\propto t$. Thus, we note

$$E_{2\,\mathrm{qp}} = 2V - O(t). \tag{6}$$

If this leads to large spatial separation of the defects, two independent quasiparticles have formed, each carrying an electric charge $-e/2$. A meaningful study of the slightly doped situation is possible only after the reference system, i.e., the undoped phase has been studied thoroughly. Therefore, in the present work we restrict ourselves to the strictly half-filled case, postponing the doped phase to a separate publication.

B. Computational considerations

Numerical results can be obtained in three different computational frame works: (i) Consideration of the Hamiltonian (1) in the full Hilbert space. While this approach is valid for all t/V, numerical calculations are possible only for rather small systems. The case $N_x \times N_y = 6 \times 4$ with 2 704 145 configurations needs already a few gigabyte storage. (ii) Restriction of the Hamiltonian (1) to the allowed subspace and 1qp-1qh states, with, e.g., 496 296 configurations for 6×6 systems with 18 fermions. In the limit of large system size, this is a severe approximation even for $t/V \ll 1$ because the possibility of having several independent vacuum fluctuations in different spatial regions is not included. This issue of size extensivity has been discussed frequently in quantum chemistry. Fortunately, it can be ignored for the systems studied in the present work. (iii) In the next section, we derive an effective Hamiltonian H_{eff} that acts only in the allowed manifold. This allows for studying much larger systems, i.e., up to 8×8 with 32 fermions and 2 891 562 configurations. This approach is intrinsically size extensive, but justified only in the large-V limit. The relation of H_{eff} and H bears some analogy to the t-J model representing the half-filled Hubbard model in the limit of large on-site repulsion and small doping.[29] The numerical effort grows exponentially with system size in all three frameworks, however much slower in (iii) than in (ii) or even (i).

C. Effective Hamiltonian

Next we derive an effective Hamiltonian $\mathcal{H}$ by downfolding the full Hamiltonian (1) so that it acts on the allowed subspace only and write it in the form

$$\mathcal{H} = H_\Sigma + H_{\mathrm{eff}}. \tag{7}$$

H_Σ comprises those contributions of H that are diagonal in the real-space basis while H_{eff} describes transitions between different allowed configurations. They lift partially the large degeneracy of the ground state when $t \neq 0$ and we are especially interested in those processes.

First consider H_Σ. To leading order in t/V one finds the *same* self-energy

$$H_\Sigma = -4\frac{t^2}{V}\sum_i n_i = -2N_xN_y\frac{t^2}{V} \tag{8}$$

for every state in the allowed subspace. This reflects the fact that in all allowed configurations each fermion has exactly four empty sites among its six nearest neighbors. H_Σ simply counts the number of possibilities to hop onto empty sites and then to return, which is the same for all states. Thus, H_Σ can be ignored for most of the following. In contrast, we show in the Appendix that for small ratios t/V any modification of the kinetic energy term in the Hamiltonian (1) leads immediately to a state-dependent H_Σ and to an insulating, charge-ordered ground state. The latter is due to an order-from-disorder mechanism. We note in passing that a state-independent second-order self-energy is found for the corresponding three-dimensional pyrochlore model as well.

Next we turn to the determination of H_{eff}. Different allowed configurations are connected through vacuum fluctuations via ring-hopping processes. The smallest ring that allows for such processes consists of six sites (hexagon) with alternating occupied and empty sites. This leads to

$$H_{\text{eff}} = -\frac{6t^3}{V^2}\left(\quad + \quad + \quad + \quad\right) + \left(\circlearrowleft \leftrightarrow \circlearrowright\right) \tag{9}$$

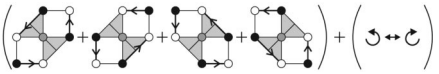

where full and empty circles denote initially occupied and unoccupied sites, respectively. The prefactor accounts for the six possible hopping orders of a given ring and given orientation. We note in passing that the corresponding amplitudes for ring-hopping processes involving four sites cancel each other for fermions, but not for bosons.[26] Ring hopping has previously been studied in magnetite,[30,31] bosonic frustrated lattice systems,[32,33] and some other strongly correlated systems such as solid helium[34,35] and the fractional quantum Hall effect.[36,37]

We can write the effective Hamiltonian (9) in the form

$$H_{\text{eff}} = t_{\text{ring}}\sum_{\hexagon} c^\dagger_{j_6}c^\dagger_{j_4}c^\dagger_{j_2}c_{j_5}c_{j_3}c_{j_1}. \tag{10}$$

The sum is over all hexagons with sites $j_1,\ldots,j_6$ and we introduced the abbreviation

$$t_{\text{ring}} = \frac{12t^3}{V^2}. \tag{11}$$

H_{eff} transforms an allowed hexagon configuration into another one when it consists of alternating occupied and empty sites.

Hopping processes on rings larger than hexagons result in prefactors of higher order in t/V. Therefore we neglect them here. The observation that each fermion hop moves the position of a τ charge over twice the distance greatly helps in the determination of the shortest paths connecting allowed configurations. Similar loops involving six alternatingly occupied and unoccupied sites constitute the effective Hamiltonian for the low-energy excitations of the corresponding three-dimensional pyrochlore model. We want to emphasize that ignoring the irrelevant energy shift H_Σ and neglecting higher-order ring-hopping processes implies that the Hamiltonian depends only on a single energy scale t_{ring}. We will see below that H_{eff} lifts the macroscopic degeneracy of the allowed states leading to a small *finite* ground-state degeneracy and a large density of states of low-energy excitations. In particular, this implies a vanishing residual entropy at $T=0$ and that higher-order processes $\sim(t/V)^k t_{\text{ring}} \ll t_{\text{ring}}$ can be expected to be irrelevant in the thermodynamic limit.

When H_{eff} is applied on an initial configuration $|i\rangle$ and the matrix element with a final configuration $|f\rangle$ is evaluated, one notices that $\langle f|H_{\text{eff}}|i\rangle$ can have different signs. It depends on whether or not the lattice site encircled by the hexagon is occupied or empty. Let us denote that site by j_0 and its occupancy by n_0. Then

$$\langle f|H_{\text{eff}}|i\rangle = (-1)^{n_0}t_{\text{ring}}. \tag{12}$$

An important question is how strongly the high degeneracy of the allowed subspace of configurations is lifted by the ring-hopping processes included in H_{eff}. In order to answer it we have to resort to numerical calculations diagonalizing H_{eff} on small systems consisting of up to $8\times 8=64$ sites.

It is found and indeed is quite obvious that H_{eff} does not couple all allowed configurations with each other, but instead does so only for subensembles. For example, stripes are not coupled by H_{eff} to any other configurations. In that case ring hopping cannot occur, and therefore those configurations are not important for the low-temperature properties of the system. One can easily convince oneself that ring hopping (9) and (10) does not change the number of particles in each row or column. Furthermore, the number of particles on the diagonals of the lattice is changed in multiples of two only and the total occupations of the two sets of criss-crossing diagonals (southwest to northeast and southeast to northwest) are left unchanged.

The fact that H_{eff} is block diagonal is enormously beneficial for numerical calculations as it allows to diagonalize each block separately. It leads to states with good transformation properties under the various discrete symmetries of the system. In order to obtain a deeper understanding of the different subensembles of allowed configurations we introduce the concept of scalar potential and topological quantum numbers.

D. Height representation and classification of subspaces

In the following we want to show that the tetrahedron rule applied to a bipartite lattice like the checkerboard one can be expressed in terms of a suitable vector field f with the discretized lattice version of curl $\mathbf{f}=\mathbf{0}$. Therefore this vector field is representable in terms of the (lattice) gradient of a scalar potential field h, i.e.,

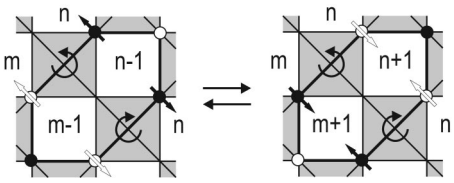

FIG. 3. Action of H_{eff} in the height representation (integer numbers on uncrossed squares). Filled (hollow) symbols signify occupied (empty) sites. Arrows and orientations are described in the text. Note that $m=n\pm1$, depending on the occupation of the central site and the orientation of the involved criss-crossed squares.

$$\mathbf{f} = \nabla h. \tag{13}$$

In order to demonstrate this we attach to each criss-crossed square an alternating orientation, i.e., a clockwise or counterclockwise one (see Fig. 3). Furthermore, a unit vector is attached to each site. This vector points in the direction of the orientation when the site is occupied, while it points in the opposite direction when the site is empty. Thus, when the tetrahedron rule is satisfied the discretized line integral around a criss-crossed square vanishes. Every integral over a closed loop in the lattice can the decomposed into integrals around criss-crossed squares. This enables us to define for each allowed configuration up to a constant a scalar potential h which satisfies Eq. (13) . For a finite lattice with periodic boundary conditions, the potential at the upper and at the lower boundary can differ only by an integer $-N_y \leqslant \kappa_y \leqslant N_y$, which is the same for all columns. The same holds true for the potential difference between the left and right side, which we call $-N_x \leqslant \kappa_x \leqslant N_x$. This defines topological quantum numbers (winding numbers). They remain unchanged by all *local* processes that transform one allowed configuration into another. Ring hopping defined by H_{eff} belongs into that category. As seen in Fig. 3, it lowers or raises merely the local potential of two plain squares by ±2. From this it follows that the subensembles of allowed configurations which block-diagonalize H_{eff} are characterized by their topological quantum numbers. This does not exclude degeneracies, i.e., several subensembles may have the same topological quantum numbers. For large system size, this is necessarily the case as the number of subensembles grows faster with increasing system size than the number of realizable (κ_x, κ_y) pairs.

We note for later reference that due to mirror symmetry there exist for each subensemble with $(\kappa_x, \kappa_y) \neq (0,0)$ three

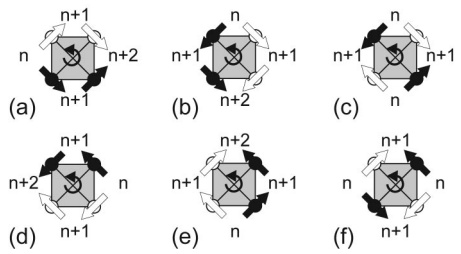

FIG. 4. The six allowed configurations of a criss-crossed square contribute differently to the average slope of h. Symbols as in Fig. 3.

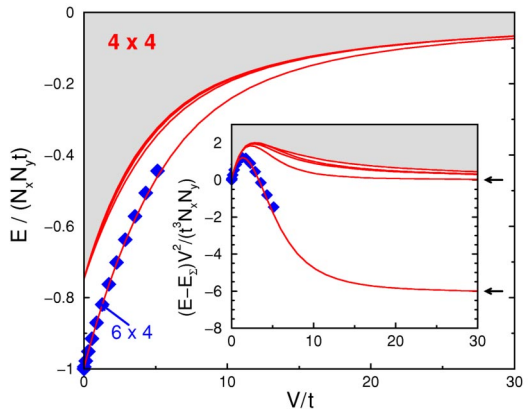

FIG. 5. (Color online) Eigenstates of the full Hamiltonian vs V/t over the full range from free fermions ($V=0$) to the limit of strong correlations ($t\to0$). Lines: Lowest 50 highly degenerate eigenvalues for system size 4×4. Energies in the gray shaded area are not shown. Symbols: Ground-state energy for system size 6×4. Inset: The t^3/V^2 contribution described by H_{eff} becomes visible after subtraction of the state-independent self-energy $E_\Sigma \equiv H_\Sigma$ and multiplication by V^2/t^3. Arrows mark the lowest eigenvalues of H_{eff}.

equivalent subensembles with $(\pm\kappa_x, \pm\kappa_y)$ and identical energies. An additional degeneracy $(\kappa_x, \kappa_y) \leftrightarrow (\kappa_y, \kappa_x)$ is found in quadratic systems, i.e., when $N_x = N_y$. Therefore, a nondegenerate ground state will necessarily have $\kappa_x = \kappa_y = 0$.

The topological quantum numbers (κ_x, κ_y) describe the average slope of the scalar potential in x and y directions. For a more detailed characterization, one may study the roughness of the potential surface, defined as the amplitude of fluctuations around the average slope. We found for the roughness of the numerically obtained ground states of H_{eff} consistently values close to 0.5.

The topological quantum numbers are intimately linked to the issue of charge ordering, discussed in more detail below in Sec. III E. This can be seen by inspection of the six local fermion arrangements depicted in Fig. 4 and their counterparts involving oppositely oriented criss-crossed squares. For the argument, assume a positive average slope of h in the thermodynamic limit, i.e., a finite positive value of κ_x/N_x. This implies that on the counter-clockwise oriented squares the first configuration in the upper row occurs more often than the first one in the lower row, and vice versa on the clockwise-oriented squares. This, in turn, implies an increased charge on every second row, i.e., horizontal stripe order. Analogously, a finite ratio κ_y/N_y implies vertical stripes. Furthermore, one can easily show that $\kappa_{x(y)}$ is the difference of the number of occupied sites and empty site on *each* row (column) taken with a sign alternating from one row (column) to the next.[38] As a consequence, all κ values are even for the boundary conditions used in this work. A pair $(\kappa_x, \kappa_y) = (0,0)$ implies that all rows and columns of the lattice contain the same number of fermions. This does not exclude diagonal stripe formation or plaquette order.

Without proof, we remark that a 1qp-1qh fluctuation is characterized by two singularities (vortex and antivortex) of the $\mathbf{f}$ field. In that case the definition of a potential requires the introduction of multiple branches or of the discretized

version of a branch cut connecting the two squares with positive and negative τ charge. Obviously, the two defects can annihilate each other again, which leads to an allowed, branch-cut-free configuration. In analogy, insertion of an additional fermion induces two equally charged vortices, which of course can not annihilate each other.

III. LOW-ENERGY EXCITATIONS

A. Comparison of H and H_{eff}

Before we discuss numerical results for H_{eff}, we substantiate the above arguments by explicit comparison of H and H_{eff} for small systems up to $6\times4=24$ sites, where a full diagonalization of the Hamiltonian (1) is possible. Figure 5 lists the lowest eigenenergies as a function of the ratio t/V. A similar energy gain per site due to the kinetic energy is seen for system sizes 6×4 and 4×4. For weak interactions $V \ll t$, energies and energy differences are of the order t. They and their degeneracies are given by the dispersion (2) evaluated for the quantized k values compatible with system size and periodic boundary conditons. With increasing interaction V, the energies regroup into the manifolds described in Sec. II A, which are separated by differences of the order of V. For $V/t \gg 1$, the energies shown in Fig. 5 are determined predominantely by H_Σ, which is the same for all states in this energy range. In order to see the physics of the large-V limit, it is useful to subtract the value of H_Σ from the energies and to multiply the difference by t_{ring}^{-1}, as displayed in the inset of Fig. 5. We notice almost constant values above $V/t \gtrsim 15$, which furthermore coincide with the results from diagonalization of H_{eff}. We conclude that in this regime the low-energy physics is describable by H_{eff}.

A numerical comparision such as the one shown in Fig. 5 allows us to estimate the parameter range where the perturbation expansion can be used. However, we note explicitly that it cannot "prove" for the infinite system the validity of the expansion underlying the derivation of H_{eff} because for finite systems perturbation theory is always valid: For sufficiently small expansion parameter, eigenvalues and low-energy subspaces will be reproduced correctly by the perturbatively derived effective Hamiltonian.

B. Participation ratio

The participation ratio (PR) of a wave function $\varphi(\mathbf{r})$ in the real-space representation is defined as

$$\mathrm{PR}[\varphi] = \frac{1}{\int |\varphi(\mathbf{r})|^4 d\mathbf{r}}. \tag{14}$$

This quantity is widely used as a measure of how localized, e.g., the eigenstates of a disordered system are. Extended states with $\varphi \sim 1/\sqrt{\Omega}$, where Ω is the system size, have a participation ratio $\sim\Omega$. Analogously, the PR of a many-particle wave function given in configuration space as superposition $|\Psi\rangle = \Sigma_\nu \alpha_\nu |\nu\rangle$ of configurations $|\nu\rangle$ can be introduced as

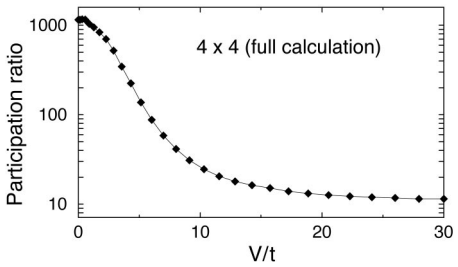

FIG. 6. Participation ratio (PR) for the full solution of a 4×4 system. Increasing particle interactions V strongly reduce the number of contributing configurations. Linear combinations with particularly low PR's were constructed within the degenerate ground-state manifold.

$$\mathrm{PR}[\Psi] = \frac{1}{\sum_\nu |\alpha_\nu|^4}. \tag{15}$$

Figure 6 demonstrates the reduction with increasing ratio V/t of the PR, i.e., the number of configurations contributing to the ground state. Clearly, increasing particle interactions strongly reduce particle-number fluctuations in real space and thus the number of real-space configurations contributing to the ground state.

For completeness, we note that the PR's of K-fold degenerate ground states $|\Psi_{\text{gs}}^{(\ell)}\rangle$, $\ell=1,\ldots,K$ are not well defined because the $\mathrm{PR}[\Psi_{\text{gs}}^{(\ell)}]$ are not invariant under unitary transformations. However, for not too large degeneracies, one can easily determine numerically the ground state $|\tilde{\Psi}\rangle$ with the smallest PR. This is done by first calculating the tensor

$$\mathcal{I}_{j_1 j_2 j_3 j_4} = \sum_\nu \alpha_\nu^{(j_1)} \alpha_\nu^{(j_2)^*} \alpha_\nu^{(j_3)} \alpha_\nu^{(j_4)*} \tag{16}$$

$(j_m=1,\ldots,K)$ and then maximizing the inverse of the PR (15),

$$(\mathrm{PR}[\tilde{\Psi}])^{-1} = \sum_{j_1,j_2,j_3,j_4}^{K} u_{j_1} u_{j_2}^* u_{j_3} u_{j_4}^* \mathcal{I}_{j_1,j_2,j_3,j_4}, \tag{17}$$

in the subspace of normalized linear combination

$$|\tilde{\Psi}\rangle = \sum_\ell u_\ell |\Psi_{\text{gs}}^{(\ell)}\rangle. \tag{18}$$

The latter is parameterized, e.g., via

$$u_1 = \cos\,\theta_1, \quad u_2 = \sin\,\theta_1 \cos\,\theta_2 e^{i\phi_2},$$

$$u_3 = \sin\,\theta_1 \sin\,\theta_2 \cos\,\theta_3 e^{i\phi_3}, \ldots, \tag{19}$$

where the angles $\theta_1, \theta_2, \ldots, \theta_K$ and $\phi_2, \ldots, \phi_K$ refer to rotations in configuration space.

C. Density of states

The low-temperature thermodynamics is determined by the low-energy excitations of the system. Therefore it is important to gain insight into their nature. As pointed out above, low-energy excitations result from lifting the high

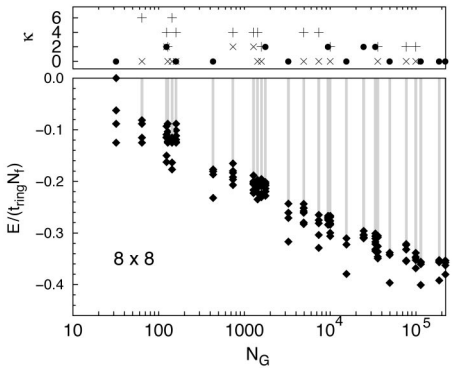

FIG. 7. Selected eigenenergies (bottom panel) and topological quantum numbers (top panel) for subensembles of states, which are connected by H_{eff}, arranged according to subensemble size N_G. Results are presented for system size 8×8 with $N_f=32$ fermions. Ten energies are shown for each subensemble as diamonds. Gray lines mark regions with eigenvalues not shown explicitly. + and × denote the larger and smaller of the values $|\kappa_x|$ and $|\kappa_y|$, respectively. Case where these coincide are indicated by ●.

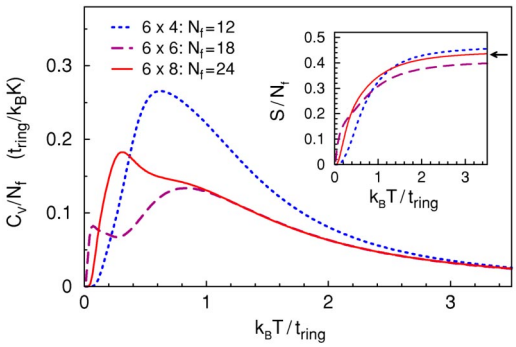

FIG. 9. (Color online) Specific heat for H_{eff} for various system sizes derived from the partition function including all allowed states. Inset: The corresponding entropies approach at high temperatures a weakly system-size-dependent value close to $2(3/4)\ln(4/3)\approx 0.43152$ per fermion (marked by an arrow).

degeneracy of the allowed configurations by H_{eff}, i.e., by ring hopping.

One expects that the effect of H_{eff} will be largest for the largest subensembles. This is confirmed by our numerical results presented in Fig. 7, which show the lowest 10 eigenenergies for each subensemble of the 8×8 system. The lowest energies always belong to states in some of the largest subensembles, but not necessarily to a state in *the* largest ones. It is interesting to look at the corresponding κ values (top panel of Fig. 7): One notices that the large subensembles tend to have small topological quantum numbers. In view of the interpretation of $\kappa_{x(y)}$ as difference of the number of occupied and empty sites in each row (column), one can expect that small κ values allow the largest number of realizations and that these allow for many ring-hopping processes. Future numerical studies can start by generating only those subensembles that have small topological quantum numbers. This greatly reduces the effort of setting up the (sparse) matrices and look-up tables needed during the diagonalization.

A measure of the low-energy excitations is the (many-body) total density of states (DOS). It is defined by

$$\rho_{\mathrm{tot}}(E)=\sum_{\ell}\delta(E-E_{\ell}), \tag{20}$$

where ℓ denotes the different eigenstates of H with eigenvalues E_{ℓ}. It is distinct from the often used single-particle DOS, which for interacting many-particle systems is defined, e.g., via Hartree-Fock eigenstates, Kohn-Sham orbitals, or in terms of quasiparticles. In particular, an approximately constant single-particle DOS ρ_0 for low-energy excitations implies an approximately exponential many-particle DOS starting at the ground-state energy E_{gs}, i.e., $\rho_{\mathrm{tot}}(E)=\theta(E-E_{\mathrm{gs}})\rho_0 e^{(E-E_{\mathrm{gs}})\rho_0}$.

The block diagonal structure of H_{eff} allows to determine *all* 94 386 eigenstates of the 8×6 system. The largest subensemble contains 8232 configurations. Figure 8 shows the resulting DOS ρ_{tot} and the corresponding number of states

$$N_S(E)=\int_{-\infty}^{E}\rho_{\mathrm{tot}}(E')dE'. \tag{21}$$

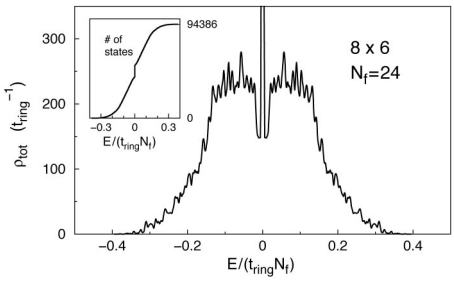

FIG. 8. Total density of H_{eff} on the 8×6 systems with $N_f=24$ fermions. $E=0$ corresponds to the energy of the system without hopping processes. Inset: Corresponding number of states N_S, clearly showing the large number of states at zero energy.

Rather striking is the behavior at $E=0$. The sharp peak of the DOS and the corresponding large step N_S result from configurations that remain uncoupled by H_{eff}, including various stripe formations. We note the very explicit $E\leftrightarrow -E$ symmetry, which is related to the symmetry $t\leftrightarrow -t$ of the half-filled case.

We always find a finite degeneracy of ground states and some charge order. Degeneracies range from twofold (6×4, 6×6, 8×6) over fourfold (10×4) and sixfold (4×4) to the eightfold degenerate case in a 10×4 lattice. In most cases horizontal or vertical stripes are seen, but plaquettes are found for the 6×6 lattice. Some of these degeneracies are protected by quantum numbers, whereas others would be lifted if instead of the lowest-order ring hopping H_{eff} the full Hamiltonian H were used. However, we expect the corresponding transition amplitudes between allowed states to become exponentially small in the thermodynamic limit, in analogy to small ferromagnetic clusters.

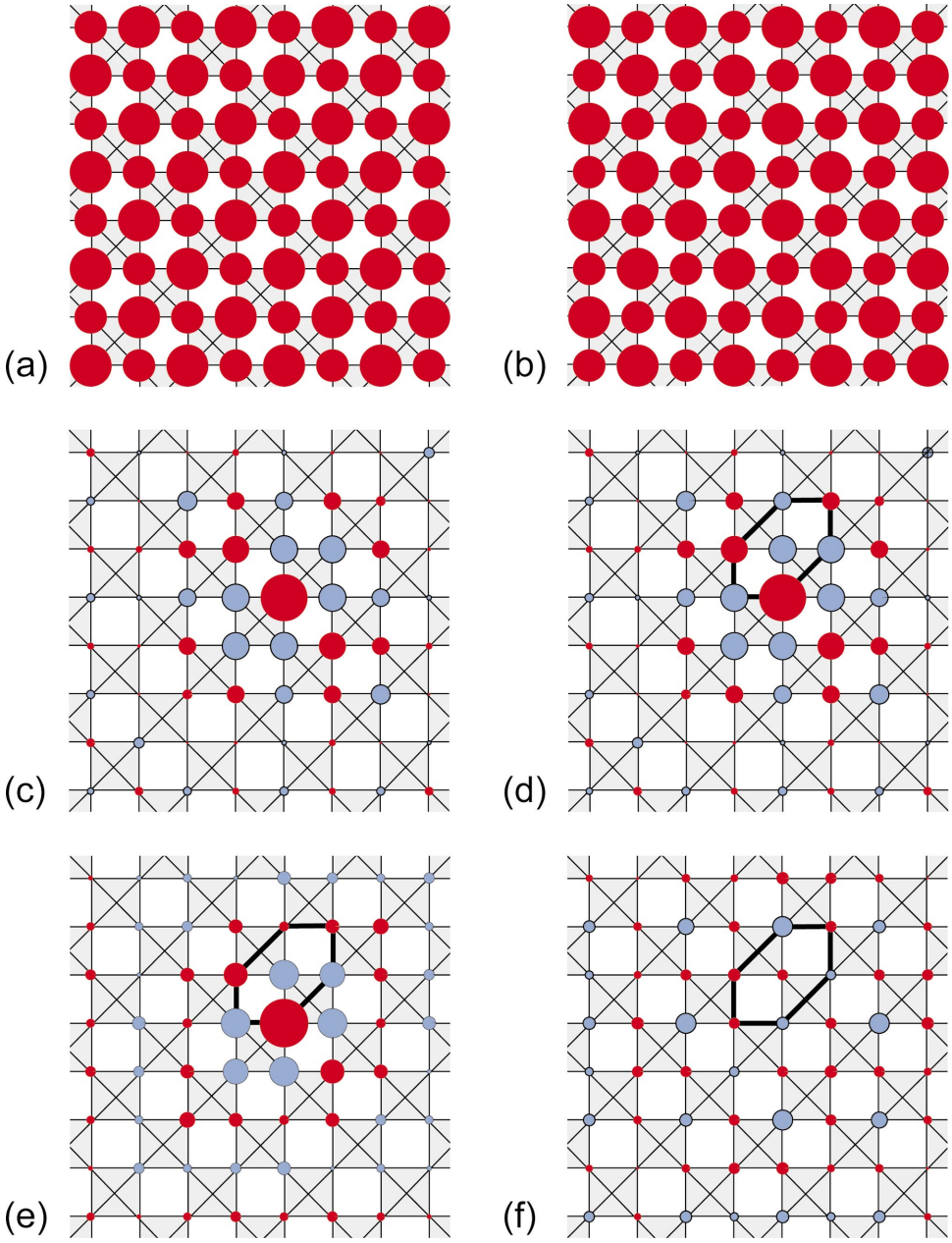

FIG. 10. (Color) (a,b) Density distribution $\langle \psi_{\rm gs}^{(\ell)} | n_i | \psi_{\rm gs}^{(\ell)} \rangle$ and (c,d) density-density correlation $\mathcal{C}_{ii_0}$, Eq. (23), for the two degenerate ground states $\ell = 1,2$ of the 8×8 system with periodic boundary conditions. The site i_0 is arbitrarily chosen [position of largest symbol in panels (c–e)]. (e) The same correlation averaged over all allowed states. (f) Difference of data from panels (d) and (e). Positive and negative values are represented by the area of dark and light colored disks, respectively. Characteristic differences between panels (d) and (e) occur along the black hexagon, which corresponds to an allowed ring-hopping process.

D. Specific heat

The low-energy excitations determine the specific heat $C(T)$ according to

$$C(T) = \frac{\partial}{\partial T} \frac{\int dE\ E \rho_{\rm tot}(E) \exp(-\beta E)}{\int dE\ \rho_{\rm tot}(E) \exp(-\beta E)}, \qquad (22)$$

where $\beta = (k_B T)^{-1}$. Numerical results for various system sizes are shown in Fig. 9. The largest systems cause a nearly linear steep increase of $C(T)$ at small T. This suggests that a large effective mass enhancement can possibly be found in frustrated lattice systems like the checkerboard lattice and possibly also the pyrochlore lattice. Note that this enhancement results from charge degrees instead of spin degrees of freedom, the usual source of heavy-fermion behavior. The entropy $(3/4)\ln(4/3) \approx 0.2158$ per site, cf. Eq. (4), is released in the temperature range $k_B T \lesssim 2t_{\rm ring}$. We expect such a large entropy release on a low-energy scale and thus a large—possibly linear—specific heat to be found in many frustrated lattice structures with charge degrees of freedom. Whether or not it will lead to a strong mass enhancement of Landau-Fermi-liquid quasiparticles must at present be left open. As pointed out Ref. 18, charged quasiparticles in frustrated lattice structures may not even form a Fermi liquid.

E. Translational invariance

We return to the issue that degenerate ground states $|\psi_{\rm gs}^{(\ell)}\rangle$ are found for all studied systems: It is suggestive to interpret this fact in terms of charge order. Charge order would imply broken translational invariance due to some order-from-

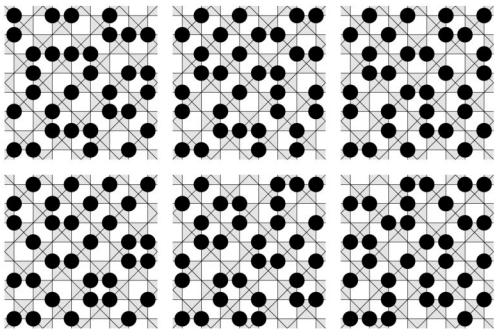

FIG. 11. Six allowed 8×8 configurations chosen randomly from the 32 states with the largest weight $|\alpha_\nu|^2\approx10^{-4}$ in one of the two degenerate ground states.

disorder mechanism analogous to the one discussed in the Appendix. Indeed, Figs. 10(a) and 10(b) show diagonal stripes in the density expectation values $\langle\psi_{\rm gs}^{(\ell)}|n_i|\psi_{\rm gs}^{(\ell)}\rangle$ of the two degenerate states $\ell=1,2$ of lowest energy in the 8×8 system. They have 20 fermions on one set of diagonals and 12 on the other (see Fig. 11 below) and are related by particle-hole symmetry as well as by other Z_2 symmetries (left-right/up-down, two sites in the unit cell).

Of course, a linear combination with homogeneous density can be constructed from these two states and furthermore topological defects will destroy possible long-range order at any finite T. But this is besides the point we want to make.

Despite the inhomogeneous density profiles of the states $|\Psi_{\rm gs}^{(\ell)}\rangle$, $\ell=1,2$, there is strong evidence that simple charge order is *not* present in the thermodynamic limit for the following arguments

(i) (a) *Different* charge-modulation patterns (horizontal and vertical stripes, diagonal stripes, plaquette order) are found for different system sizes, whereas one should expect to find the *same* pattern for all large enough systems if the thermodynamic limit led to a charge-ordered state.

(i) (b) The amplitude of the charge modulation decreases with system size (not shown). We reiterate that a finite (small) topological quantum number $\kappa_{x(y)}$ necessarily implies a (weak) charge modulation $\sim\kappa_{x(y)}/N_{x(y)}$. Note that in finite systems charge modulation is observed even for free fermions if the Hamiltonian is diagonalized in a standing-wave basis. Unfortunately in contrast to that simple case, for the Hamiltonian of interest here a reliable extrapolation to an infinite system is not possible because the charge-modulation pattern varies too much from one system size to another.

(ii) Consider the case of complete order corresponding, e.g., to Fig. 10(a). All lower-left and upper-right sites in the criss-crossed squares are occupied while the remaining sites are empty. This state does *not* gain energy within the effective-Hamiltonian approximation because no ring-hopping processes are possible. The same holds true for the other completely charge-ordered stripe configurations.

(iii) (a) The participation ratio of the ground states, i.e., the approximate number of configurations contributing significantly to it, is very large: $\mathrm{PR}[\Psi_{\rm gs}^{(\ell)}]=46919.3$.

(iii) (b) There is no single reference configuration that has the largest weight, but instead 32 configurations ν have each $|\alpha_\nu|^2=1.18\times10^{-4}$. Six of them are shown as Fig. 11 for better illustration. They clearly look like one visualizes "generic" allowed states and not like charge-ordered configurations.

(iv) More evidence for a liquidlike behavior, i.e., the absence of broken translational symmetry in the infinite systems, is provided by the density-density correlation function

$$C_{ii_0}=\langle\psi_{\rm gs}^{(\ell)}|n_in_{i_0}|\psi_{\rm gs}^{(\ell)}\rangle-\langle\psi_{\rm gs}^{(\ell)}|n_i|\psi_{\rm gs}^{(\ell)}\rangle\langle\psi_{\rm gs}^{(\ell)}|n_{i_0}|\psi_{\rm gs}^{(\ell)}\rangle \quad (23)$$

shown in Figs. 10(c) and 10(d). Qualitatively the same behavior is found for all system sizes and all degenerate ground states (not shown). Note that panels (c) and (d) show the correlations of inequivalent sites, with the center i_0 in one case having on average an occupation larger than 0.5 and in one case less than 0.5.

The correlations in the quantum ground states are best understood as reflecting the algebraic correlations present in the classically degenerate allowed manifold. They are the sum of the correlations of *all* allowed configurations with equal weight and are shown in Fig. 10(e). Specific quantum-mechanical features resulting from the ring hops become visible by determining the difference of the actual correlations of panel (d) and the classical correlations (e). This is shown as panel (f). A negative value at the central site i_0 indicates the expected general reduction of fluctuations compared to the generic value. A closer look reveals further differences along, e.g., the six-site loop marked in the figure. In contrast to the "classical correlations" in panel (e), the ground-state correlations (d) have alternating signs. This is not surprising, but merely reflects the fact that alternations of occupied and empty sites is necessary for ring hopping and thus lowering of the energy.

In view of (i)–(iv), we expect the charge order to be a finite size effect and to vanish in the thermodynamic limit leading to a twofold degenerate, translational invariant ground state. However, any conclusion drawn from exact diagonalization of finite clusters has to be considered with caution as unexpected features may arise in the thermodynamic limit. In general, exact diagonalization studies have to be combined with interpretations obtained by other methods and finally have to be compared to experiment.

IV. CONCLUSION AND OPEN QUESTIONS

The aim of this paper is to achieve a better understanding of charge degrees of freedom in frustrated lattice structures. As a first step in this direction we have studied here the ground state of a spinless fermion model on a checkerboard lattice at half filling. The Hamiltonian (1) presents in our view the simplest model by means of which one can investigate the interplay between a macroscopically degenerate fermionic ground-state manifold due to particle-particle interactions and a kinetic energy term. In a previous investigation[18] this model and a generalization of it including spin were predicted to have highly unusual properties—most noticeably quasiparticles with a fractional charge of $\pm e/2$ and a spin smeared over parts of the sample. These observations have been made for an average of 0.5 fermions per site.

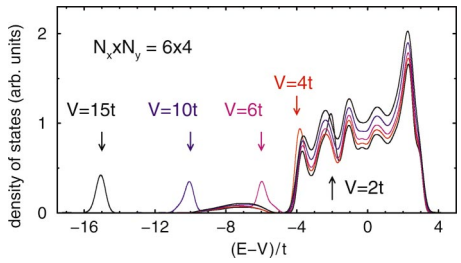

FIG. 12. (Color) Density of states ρ_{tot} restricted to the Hilbert space spanned by allowed states and the 1qp-1qh states. In order to keep the broad band of predominantly 1qp-1qh character at fixed position, ρ_{tot} is plotted versus $E-V$. This moves the position of the allowed states dressed by 1qp-1qh fluctuations to $(E-V)/t=-V/t$ (marked by arrows).

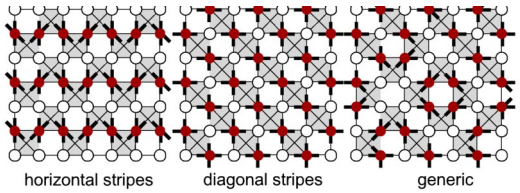

FIG. 13. (Color online) Illustration of the second-order contributions to the self-energy H_{Σ} for some allowed configurations. Filled (hollow) symbols signify occupied (empty) sites. Short solid lines indicate directions of possible hops. States with horizontal and vertical (diagonal) stripe order have less (more) *diagonal* nearest-neighbor pairs than any generic configuration.

An equally fascinating prediction, namely spin-charge separation, has been made for frustrated lattices with almost all sites occupied by one electron.[8,32,39]

The numerical results presented here suggest a translational invariant "disordered" ground state for the checkerboard lattice with possibly a finite, geometry-dependent degeneracy. In fact, we expect in the thermodynamic limit a twofold degenerate state. Future numerical studies with more powerful computers than the one available to us on larger systems and different geometries should allow for confirming or disproving this proposition. They also should help to clarify the relation to the concept of topological order[41,42] as introduced by Wen and Niu[43] and to the fractional quantum Hall effect.[36,37]

We showed that the entropy associated with the original macroscopic degeneracy is released on an energy scale $t_{\mathrm{ring}}=12t^3/V^2$, which for $t \ll V$ is much smaller than the underlying energy t. Note that the ring hopping described by H_{eff} does not lead to charge transport since the center of mass of the involved fermions remains unchanged.

Better insight into the lifting of the degeneracy was obtained with the help of the height representation, which led to the introduction of topological quantum numbers. Based on our calculations, we expect the ground state to have a flat height function and topological quantum numbers $(\kappa_x,\kappa_y) \approx (0,0)$ because they allow for the largest number of allowed configurations.

This brings us back to the issue of the metal-insulator transition expected at a finite value $V/t=O(1)$. It can be studied only by taking into account the full Hilbert space, i.e., within level (i) of Sec. II B. On this level, we were able to study only rather small systems that furthemore exhibit some artefacts since even small loops can span across the entire system. Neither the energies in Fig. 5 nor the corresponding participation ratios in Fig. 6 give any indication of a nonanalytic behavior signaling a phase transition at finite V/t.

Indications of the position of the metal-insulator transition can be obtained on level (ii) of Sect. II B, i.e., in a calculation comprising the allowed states and the 1qp-1qh states. For strong interactions, the density of states curves shown in Fig. 12 consist each of a narrow peak and a broad band separated by about $V-4t$. The former results from the allowed states dressed by 1qp-1qh fluctuations, including those which lead to H_{Σ} and H_{eff}. For large ratios V/t, width and shape of this peak should be close to $\rho_{\mathrm{tot}}(E)$ in Fig. 8. These details are smeared out in Fig. 12 due to numerical broadening. The broad band near $E=V$ is made primarily of states that violate the τ rule twice. As discussed above, these defects are mobile and probably deconfined. Indeed, a width proportional to t is observed. Note that the approximation (ii) looses its validity when V/t is small enough so that many qp-qh pairs are created, i.e, near the expected insulator to metal transition. Nevertheless, one can take the range $V/t \approx 4-10$ where the two features begin to overlap as estimation for the position of the quantum phase transition. This estimation coming from the large-V side can be supplemented by mean-field estimations coming from the small-V side, which yield similar values.[44] A detailed description of the transition itself is at present beyond our numerical possibilities.

In the language of the height representation, the expected metal-insulator transition corresponds to a proliferation of vortex-antivortex pairs. The system would change from one translational invariant state to another, probably with a transition of Kosterlitz-Thouless type. Such transitions are notoriously difficult to study numerically.

Having gained some insight into the ground state with the help of topological numbers, the present work needs extension in several directions. First there is the problem of doping, which should yield fractionally charged excitations. Obviously, a detailed understanding of the undoped reference state as initiated by the present work is a prerequiste for the study of (weakly) doped systems. Then there is the introduction of the spin, which needs further elucidation. A very unusual kind of physics is expected here, because the breaking up of a charge e into $2\times e/2$ has drastic consequences for the spin.[18,40] Last but not least it is challenging to study how the field theory for the present system with the extensions just described fits into a more general framework of existing field theories, in particular lattice gauge theories.[45] So a considerable amount of work remains to be done.

ACKNOWLEDGMENTS

We thank K. Penc, N. Shannon, and A. Langari for discussions on the diagonalization of small frustrated lattice systems. We also acknowledge helpful remarks

by K. Becker, J. Betouras, R. Moessner, P. Thalmeier, V. Yushankhai, and Y. Zhang.

APPENDIX: ORDER FROM DISORDER IN MODIFIED MODELS

For a better understanding of the subtle particularities of the checkerboard model, we introduce in this Appendix different hopping amplitudes t' and t for diagonal and other hopping, respectively. The second-order self-energy (8) for a configuation with P_{diag} diagonal nearest-neighbor pairs is

$$H_{\Sigma} = -N_x N_y \frac{t^2 + t'^2}{V} - 2P_{\mathrm{diag}} \frac{t^2 - t'^2}{V}. \tag{A1}$$

This favors, depending on relative order of the magnitudes of t and t', either horizontal/vertical or diagonal stripe order, which minimizes or maximizes the number of diagonal pairs and thereby their contribution to the energy gain by quantum fluctuations. This simple order-from-disorder mechanism is illustrated in Fig. 13.

[1] *Proceedings of the Conference on Highly Frustrated Magnetism 2003*, 26–30th August 2003, Grenoble, France; special issue J. Phys.: Condens. Matter 16 (11) (2004).

[2] *Frustrated Spin Systems*, edited by H. T. Diep (World Scientific, Singapore, 2004).

[3] G. Misguich and C. Lhuillier, in Ref. 2, cond-mat/0310405 (unpublished).

[4] R. Moessner and S. L. Sondhi, Phys. Rev. B **63**, 224401 (2001).

[5] R. Moessner, S. L. Sondhi, and E. Fradkin, Phys. Rev. B **65**, 024504 (2002).

[6] W. Brenig and A. Honecker, Phys. Rev. B **65**, 140407 (2002).

[7] J.-B. Fouet, M. Mambrini, P. Sindzingre, and C. Lhuillier, Phys. Rev. B **67**, 054411 (2003).

[8] A. Läuchli and D. Poilblanc, Phys. Rev. Lett. **92**, 236404 (2004).

[9] See, e.g., N. Tsuda, K. Nasu, A. Fujimori, and K. Siratori, *Electronic Conduction in Oxides*, 2nd ed. Vol. 94 of Springer Series Solid-State Sciences (Springer, Berlin, 2000).

[10] E. J. W. Verwey and P. W. Haayman, Physica (Amsterdam) **8**, 979 (1941).

[11] H. Takagi (private communication); see also Bull. Am. Phys. Soc. **48** (1), 140 (2003).

[12] K. Matsuno, T. Katsufuji, S. Mori, M. Nohara, A. Machida, Y. Moritomo, K. Kato, E. Nishibori, M. Takata, M. Sakata, K. Kitazawa, and H. Takagi, Phys. Rev. Lett. **90**, 096404 (2003).

[13] S. Kondo, D. C. Johnston, C. A. Swenson, F. Borsa, A. V. Mahajan, L. L. Miller, T. Gu, A. I. Goldman, M. B. Maple, D. A. Gajewski, E. J. Freeman, N. R. Dilley, R. P. Dickey, J. Merrin, K. Kojima, G. M. Luke, Y. J. Uemura, O. Chmaissem, and J. D. Jorgensen, Phys. Rev. Lett. **78**, 3729 (1997).

[14] For a review of theoretical work, see P. Fulde, J. Phys.: Condens. Matter **16**, S591 (2004).

[15] E. J. W. Verwey, Nature (London) **144**, 327 (1939).

[16] P. W. Anderson, Phys. Rev. **102**, 1008 (1956).

[17] I. Leonov, A. N. Yaresko, V. N. Antonov, M. A. Korotin, and V. I. Anisimov, Phys. Rev. Lett. **93**, 146404 (2004).

[18] P. Fulde, K. Penc, and N. Shannon, Ann. Phys. (Leipzig) **11**, 892 (2002).

[19] E. H. Lieb and P. Schupp, Phys. Rev. Lett. **83**, 5362 (1999).

[20] S. E. Palmer and J. T. Chalker, Phys. Rev. B **64**, 094412 (2001).

[21] B. Canals, Phys. Rev. B **65**, 184408 (2002).

[22] S. Fujimoto, Phys. Rev. B **67**, 235102 (2003).

[23] O. Tchernyshyov, O. A. Starykh, R. Moessner, and A. G. Abanov, Phys. Rev. B **68**, 144422 (2003).

[24] E. Berg, E. Altman, and A. Auerbach, Phys. Rev. Lett. **90**, 147204 (2003).

[25] J.-S. Bernier, C.-H. Chung, Y. B. Kim, and S. Sachdev, Phys. Rev. B **69**, 214427 (2004).

[26] N. Shannon, G. Misguich, and K. Penc, Phys. Rev. B **69**, 220403 (2004).

[27] A. Mielke, J. Phys. A **24**, L73 (1991); **24**, 3311 (1991).

[28] E. H. Lieb, Phys. Rev. Lett. **18**, 692 (1967).

[29] See, e.g., Chap. 12.6 of P. Fulde, *Electron Correlations in Molecules and Solids*, 3rd ed. (Springer, Heidelberg, 1995).

[30] J. R. Cullen, Philos. Mag. B **42**, 387 (1980).

[31] S. Iida, Philos. Mag. B **42**, 349 (1980).

[32] L. Balents, M. P. A. Fisher, and C. Nayak, Int. J. Mod. Phys. B **12**, 1033 (1998).

[33] A. Paramekanti, L. Balents, and M. P.A. Fisher, Phys. Rev. B **66**, 054526 (2002).

[34] D. J. Thouless, Proc. Phys. Soc. London **86**, 893 (1965).

[35] B. Bernu and D. M. Ceperley, J. Phys.: Condens. Matter **16**, S701 2004.

[36] S. Kivelson, C. Kallin, D. P. Arovas, and J. R. Schrieffer, Phys. Rev. Lett. **56**, 873 (1986).

[37] D. J. Thouless and Q. Li, Phys. Rev. B **36**, 4581 (1987).

[38] J. Betouras (private communication).

[39] T. Senthil and M. P. A. Fisher, Phys. Rev. B **62**, 7850 (2000).

[40] K. Penc and N. Shannon (private communication).

[41] X.-G. Wen, Phys. Rev. B **65**, 165113 (2002).

[42] M. Freedman, C. Nayak, and K. Shtengel, cond-mat/0312273 (unpublished).

[43] X.-G. Wen and Q. Niu, Phys. Rev. B **41**, 9377 (1990).

[44] Y. Zhang (private communication).

[45] J. B. Kogut, Rev. Mod. Phys. **51**, 659 (1979).